metals

MDPI

Article

Understanding the Role of β Recrystallization on β Microtexture Evolution in Hot Processing of a Near-β Titanium Alloy (Ti-10V-2Fe-3Al)

Dayu Shu [1,*], Li Wang [2,3], Qiang Chen [1], Yi Yao [2,3], Minghui Li [2,3] and Rui Wang [2,3]

[1] Southwest Technology and Engineering Research Institute, Chongqing 400039, China; chenqiang59@yeah.net
[2] State Key Laboratory of Solidification Processing, School of Materials Science and Engineering, Northwestern Polytechnical University, Xi'an 710072, China; wangli_coffe@126.com (L.W.); yaoyi@mail.nwpu.edu.cn (Y.Y.); 1eemh@mail.nwpu.edu.cn (M.L.); rwang@mail.nwpu.edu.cn (R.W.)
[3] Shaanxi Key Laboratory of High-Performance Precision Forming Technology and Equipment, Northwestern Polytechnical University, Xi'an 710072, China
* Correspondence: shudayu1980@163.com

Abstract: The present study evaluated the β recrystallization behavior and deformation microtexture evolution of TB6 titanium alloy (Ti-10V-2Fe-3Al) taking place during isothermal compression. The hot deformation tests were carried out in the temperature range below the β phase transition temperature and spanned a wide strain rate range of 0.0001~1 s^{-1}. Microstructure evolution on β phase, including its recrystallization behavior and microtexture formation, is sensitive to the strain rates, whereas the average grain size of equiaxed α phase exhibits a slight increase with the strain rate decreasing. Moreover, β recrystallization is not homogeneous among the prior β grains, and is characterized by: (I) enriched β sub-grains, (II) sporadically or chain-like distributed recrystallized β grains with a grain size far less than the prior β grains, and (III) wave-shaped β grain boundaries. The β recrystallization is inadequate and its orientation takes on the inheritance characteristic, which makes the β microtexture significant after deformation. At a lower strain rate, the high activity of the {11−2}<111> and {12−3}<111> slip systems induced the crystal rotation around <101>, but such crystal rotation did not destroy the Burgers orientation relationship (BOR), which could be accounted for by the generation of a strong microtexture of <001>//RD. The divergences on β recrystallization fraction, the operation of slip systems, and initial crystal orientations explain the different microtexture components with varied intensities under different deformation conditions.

Keywords: hot deformation; dynamic recrystallization; β microtexture; near-β titanium alloy

Citation: Shu, D.; Wang, L.; Chen, Q.; Yao, Y.; Li, M.; Wang, R. Understanding the Role of β Recrystallization on β Microtexture Evolution in Hot Processing of a Near-β Titanium Alloy (Ti-10V-2Fe-3Al). *Metals* **2021**, *11*, 1397. https://doi.org/10.3390/met11091397

Academic Editor: Francesca Borgioli

Received: 31 July 2021
Accepted: 26 August 2021
Published: 3 September 2021

1. Introduction

Near β titanium alloy serves as an important structural material with high strength, low weight, and excellent corrosion resistance, and these important property features make the material one of the most potential candidates for wide application in various fields such as aerospace, automotive, and weaponry and equipment industries [1–4]. Compared with other materials with high performance, it shows significant advantages on strength, corrosion resistance, biocompatibility, and formability [3,5–7]. For the specific use of the alloys, they would undergo multiple processing procedures to achieve the required shape of the component. Generally, radical plastic deformation, like forging and hot rolling deformation, is an essential step in the component forming process [8]. Simultaneously, the required mechanical properties can be directionally modulated during hot working by means of the sensibility of microstructure evolution on processing variables [9–11], finally yielding a desirable Ti-alloy product with minimal scrap. Therefore, a comprehensive and profound understanding of the behavior and intrinsic mechanisms of the microstructure transformation and crystallographic texture evolution that determine the performance of products is a prerequisite for working out the proper processing craft route.

A homogeneous microstructure without significant preferred grain orientation is an eternal pursuit, especially for the forming of a large-scale structural component. However, it is difficult for near-β titanium alloys, which is mainly reflected in the coarse β grains that are hard to refine and the β microtexture generated after hot deformation. For the texture, which is directly influenced by thermo-mechanical processing (TMP), its components and evolution rules may be associated with phase transformation, lamellar morphology transformation, and recrystallization behavior. The result is that a cluster of α phase with a sharp orientation concentration named macrozone would generate, which can be observed in the billets of near-α titanium alloy [12,13]. Such a local α texture can be weakened to a certain extent via changing the strain path and adopting the interrupted loading method to accelerate the α morphology transformation and improve the microstructure homogeneity [14,15]. However, for the β titanium alloys forged in single β phase regime, they usually showed a sharp {001} texture, i.e., the {001} crystal planes of β phase were perpendicular to loading direction [16]. The dynamic recrystallization (DRX) and dynamic recovery (DRV) mainly control the microstructural evolution during hot deformation in single β phase regime. Differently, the fiber textures of {001} and {111} are generated during (α + β)-phase field deformation [17]. Therefore, we can conclude that the β texture generated in deformation or post-deformation treatment and its intensities may be significantly affected by the processing parameters, α phase evolution, and β recrystallization.

Over the past years, abundant investigations on hot deformation of typical near-β titanium alloy, such as Ti-55531 alloy, Ti-7333 alloy, and Ti-1023 alloy, have been made by researchers [8,18–23]. It has been generally accepted that DRV and DRX serve as the primary dominant mechanisms controlling the isothermal compression process in a single β phase field and (α + β) dual-phase field. Additionally, the two microstructure evolution behaviors are all sensitive to the deformation temperature, strain rate, strain, and phase transformation [18–22]. The investigations by Chen et al. [23] and Murty et al. [24] demonstrated that the DRX that occurred in rolling deformation was an effective mechanism for grain refinement, which can weaken the intensities of deformation texture to some extent. In continuous cooling hot deformation, the β DRX also played an important role in weakening the texture, where the texture components differed at different cooling rates. The above research provides us with an extensive understanding of the characteristics of β phase evolution and its influence in weakening the deformation texture. However, the experimental results by Li et al. [8] showed that recrystallization texture would inherit the texture components of the deformed matrix, i.e., the nucleation sites of recrystallized grains could be selective. They held the view that the strain-induced boundary migration (SIBM), as a typical mechanism for the static mechanism, mainly controlled the recrystallization behavior during the hot-rolling deformation followed by the air-cooling process. Therefore, considering the multiple mechanisms controlling the DRX process, it can be concluded that the deformation texture is strongly associated with β recrystallization behavior. In addition, Meng et al. [16] and Li et al. [25] hold a view that β phase evolution was significantly affected by α kinking or α precipitation. Generally, in practical industrial production, the processing route of hot forging in the (α + β) phase field is of vital importance to modulate the mechanical properties of titanium alloys. The α phase microstructure evolution, including its morphology transformation and phase transformation, would affect the β phase evolution. During deformation, α coarsening with its grain boundaries expanding could be observed, especially at a lower strain rate, which would affect the lattice rotation and the dislocation gliding in the neighboring β phase. Both would affect the dynamic recovery and continuous recrystallization, and consequently, the microtexture evolution. However, for the hot processing in the (α + β) dual-phase regime, limited literature is available elucidating the role of β recrystallization on β microtexture evolution.

It can be concluded that the understanding of β recrystallization and β microstructure evolution is of vital importance to develop and enrich the mechanisms in the hot deformation of titanium alloys. In addition, from the industrial point of view, it would be helpful to explore a more effective technological route for grain refinement and texture

control. Therefore, this paper aims at deepening understanding of the β microtexture formation mechanism by considering multi-mode microstructural evolution including α phase and β phase evolution. We paid specific attention to the role of β recrystallization on β microtexture characteristics. Considering that the TB6 (Ti-10V-2Fe-3Al) is a typical near-β titanium alloy and its practical application is relatively wide, it was thus selected for this investigation. In this paper, the forged TB6 (Ti-10V-2Fe-3Al) bar with equiaxed α grains was used, and the hot compression was carried out in the (α + β) dual-phase regime. The electron backscatter diffraction (EBSD) technique was used to analyze the crystallographic orientations and microstructural morphology. The conclusions explain a deeper understanding of the complicated microstructure evolution during hot deformation of near-β titanium alloys, providing further instructions on the determination of hot processing parameters.

2. Materials and Methods

A hot forged bar of TB6 titanium alloy with a diameter of 350 mm was used as the initial material in this research, which was produced by Western Superconducting Technologies Co., Ltd. (Xi'an, China) Based on the multiple measurements, the chemical composition (in wt. %) of the as-received bar was determined to be 9.92V, 1.79Fe, 3.23Al, 0.007C, 0.005N, 0.102O, and Ti (balance). By means of metallographic method, the $\alpha \rightarrow \beta$ transition temperature was examined to be 805 °C. Further, some standard samples with the height of 12 mm and the diameter of 8 mm were prepared for the subsequent isothermal compression tests. Hot compression tests in this paper were all conducted on a Thermecmaster-Z thermal-mechanical simulator, which works under a certain vacuum environment. The key factor that matters for the success of hot compression tests lies in the control and measurement of sample temperatures. Therefore, the R-type thermocouple was chosen and two thermocouple wires were needed in our compression tests. At the center of the height of the cylindrical specimen, the two thermocouples were welded onto the side surface of the sample and they were next to each other. Furthermore, the friction between the specimen and dies is also inescapable. Therefore, two pieces of mica plates were required to be placed in advance on the bottom and top surfaces of the compression specimens, respectively, with the purpose of reducing friction and achieving a relatively uniform deformation during compression.

The hot compression tests were performed at the temperature ranging from 740 °C to 780 °C with a 20 °C interval and the strain rates of 0.0001 s^{-1}, 0.01 s^{-1}, and 1 s^{-1}. The compression ratio at each deformation condition was 50% in the vertical direction of the specimen. The specimen was required to be held for 5 min at the deformation temperature for the purpose of ensuring the uniform temperatures distribution on the specimen before deformation. After deformation, argon gas would flow onto the compressed specimen to achieve the fast cooling of specimens, thereby retaining the as-deformed microstructure.

The compressed specimen was cut axially for further microstructure characterization. The microstructure was examined by the Lecia DMI3000M optical microscope (LECIA, Shanghai, China) and the ZEISS Sigma 300 scanning electron microscope (ZEISS, Shanghai, China) with a Nordlys Nano Detector. The EBSD samples were prepared by conventional grinding and finally polished on a BUEHLER vibratory finishing machine (BUEHLER, Shanghai, China). For EBSD examination, the selected observation areas were located in the center of the samples, and the step size was 0.4–1.5 μm. The data acquisition was post-processed using HKL Channel 5 EBSD software (veision 5.0.9.0, Oxford Instruments, Oxford, UK) and the non-commercial imaging software ATEX© (version 2.14, Université de Lorraine, Metz, France) [26].

3. Result and Discussion

3.1. The Microstructural Characteristics of the As-Received Material

It can be seen from Figure 1a that the microstructures of the as-received TB6 bar are bimodal with 67% equiaxed α grains uniformly embedded in a β matrix. It was a forged

billet experiencing multiple forging/annealing loading routines in single β and dual (α + β) domains. The average size of equiaxed α grains was near 3 μm. Figure 1b indicates the orientation map of the β phase in a cross-section microstructure. It can be seen that the local texture of the β phase is significant according to the orientation distribution of the β phase. The β microstructure is commonly found in the deformed near-β titanium alloy [27].

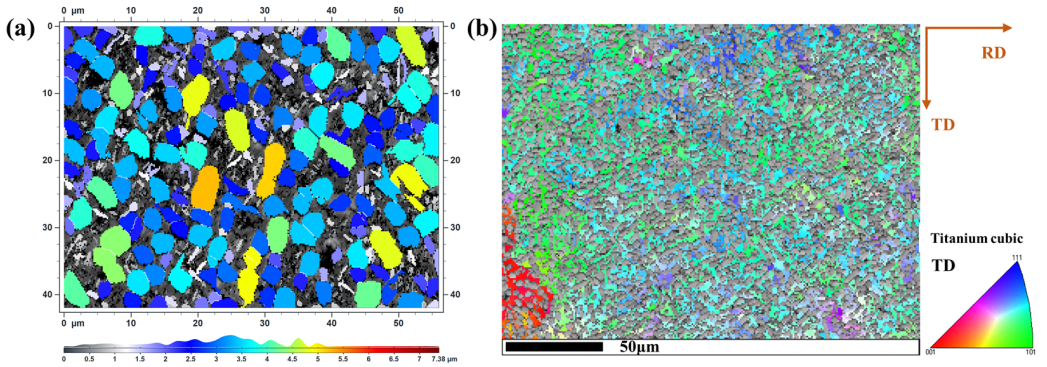

Figure 1. (**a**) α grain sizes distribution map; (**b**) the inverse pole figure (IPF) map of the β phase of the as-received TB6 alloy.

The DRV is the dominant soft mechanism during hot deformation for the titanium alloys with high stacking fault energy [28]. The DRX, as an effective way of grain refinement, could be promoted to some extent by increasing the deformation temperature and decreasing the strain rate [29]. However, the contribution of the recrystallization fraction of the β phase to the refinement of the β phase is still limited. In addition, the generation of recrystallization grains may lead to the strengthening of the local β texture. Generally speaking, it is hard to effectively weaken the β microtexture by hot working. However, α texture intensity can be effectively controlled by means of its morphology transformation. According to our previous studies [14], the α morphology transformation process (globularization) can be accelerated by multi-pass interrupted loading and multi-directional loading. Synchronously, considering the sensitivity of the lamellar α evolution to its geometric and crystallographic orientations and the semi-quantitative relationship between them [15], the α texture could be directionally regulated. However, based on the abundant studies [27], it can be concluded that a {110} β pole would overlap the {0001} α pole, but with significant spread after hot processing. It reflected the remaining trace of the Burgers orientation relationship. Consequently, the deformed β grains still tend to present a local orientation concentration, which is hard to eliminate simply by hot working.

3.2. The As-Deformed Microstructure

3.2.1. The Effects of Strain Rates and Deformation Temperatures on the Morphology and Distribution of the Prior α Phase

Figures 2 and 3 exhibit a general view of the deformed α phase microstructural characteristics. The characterization results indicate that the α phase distribution, including its morphology, grain size, and volume fraction, is uniform for the initial microstructure, which can be seen in Figure 2a (the white phase denotes the α phase). After deformation, overall, the α phase distribution remains relatively homogeneous in center deformation regions, as shown in Figure 2b–f. However, due to the small grain size of the α phase and the limitations of metallographic images, it is hard to further identify some important information about the α morphology, its distribution features, and the grain size. Therefore, the corresponding EBSD data were also analyzed, as shown in Figure 3. It can be seen that the grain size of the equiaxed α phase is 2–4 μm and it has a slight increase with the strain rate decreasing. However, the volume fraction of the α phase would decrease significantly with the deformation temperature increasing (Figure 3f). In addition, the volume fraction of the α phase is not sensitive to the strain rate. By contrast, the deformation temperature mainly affects the α → β phase transformation process, but has little influence on α

phase coarsening. According to the investigation by Lin et al. [30], as the strain rates or deformation amounts increased, the volume fraction of the α phase would decrease. They contributed this phenomenon to the dynamic transformation during hot deformation; however, it is not observed in the experimental results in this work.

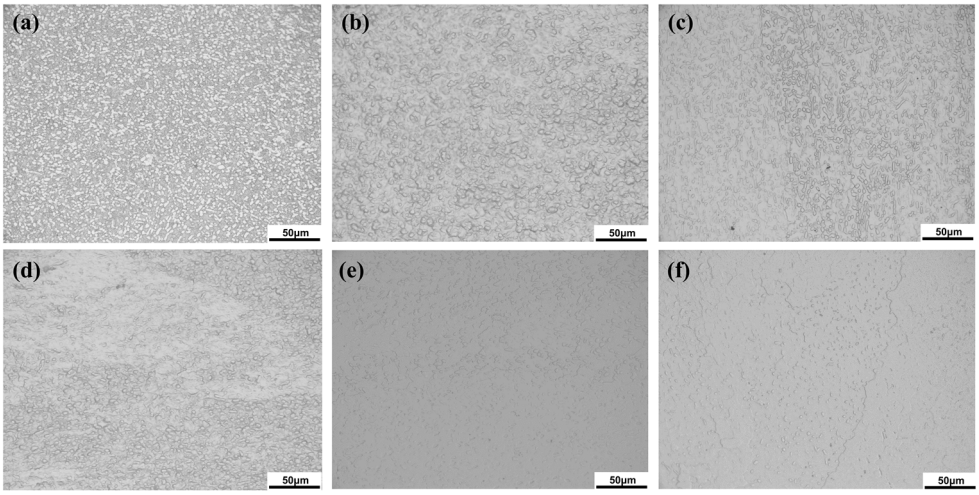

Figure 2. The metallographic cross-sections of TB6 alloy at different conditions: (**a**) the as-received material; (**b**) 740 °C/0.0001 s^{-1}; (**c**) 740 °C/0.01 s^{-1}; (**d**) 740 °C/1 s^{-1}; (**e**) 760 °C/0.0001 s^{-1}; (**f**) 780 °C/0.00001 s^{-1}.

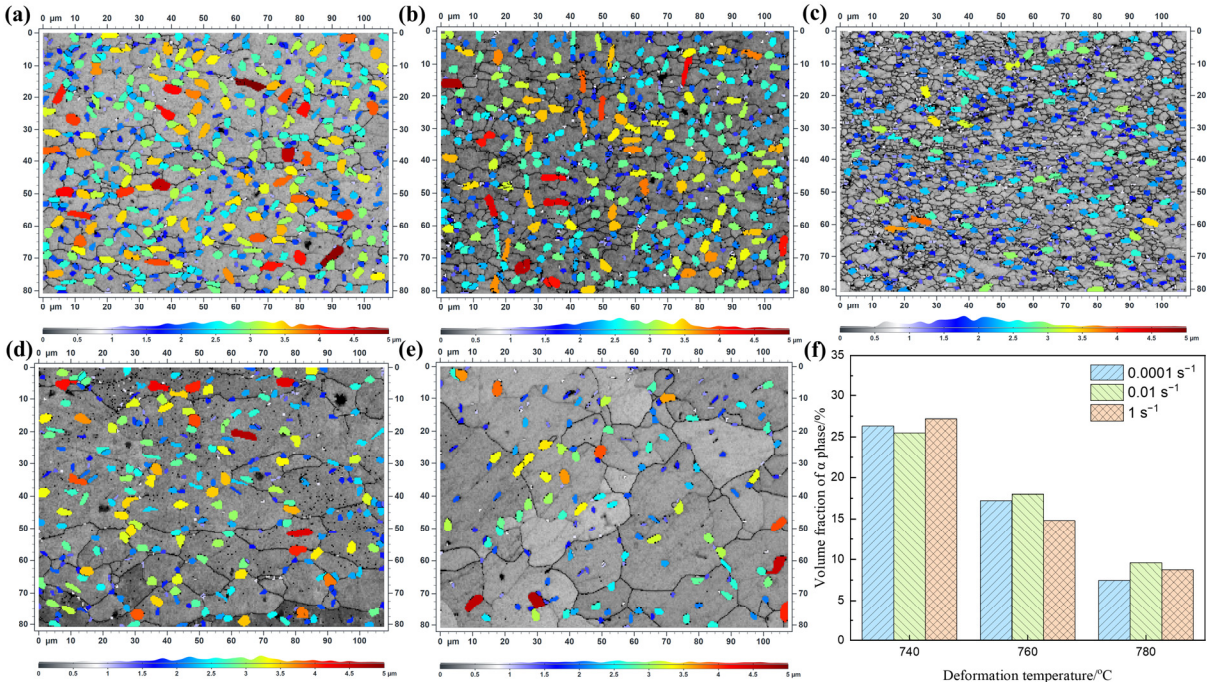

Figure 3. The α grain sizes spread under different deformation conditions: (**a**) 740 °C/0.0001 s^{-1}; (**b**) 740 °C/0.01 s^{-1}; (**c**) 740 °C/1 s^{-1}; (**d**) 760 °C/0.0001 s^{-1}; (**e**) 780 °C/0.0001 s^{-1}; and (**f**) the variation of α volume fraction with deformation conditions.

The α phase evolution is further analyzed by incorporating the crystallographic and morphologic information. Figure 4 shows the IPF maps of the α phase and the corresponding distribution of grain boundary misorientation in the α phase of the deformed microstructure at different deformation conditions. It is worth noting that the high-angle grain boundaries (HAGBs) occupy the certain proportion at the strain rate of 0.0001 s^{-1}, as

shown in Figure 4a,d,e. The fractions of low-angle grain boundaries (LAGBs) in the α phase are higher than that of the HAGBs at the strain rates of 0.01 s^{-1} and 1 s^{-1}, as indicated in Figure 4b,c. The result indicates that the deformation would make new LAGBs and HAGBs in equiaxed grains. Additionally, the generation of LAGBs would be accelerated with the stain rate increasing.

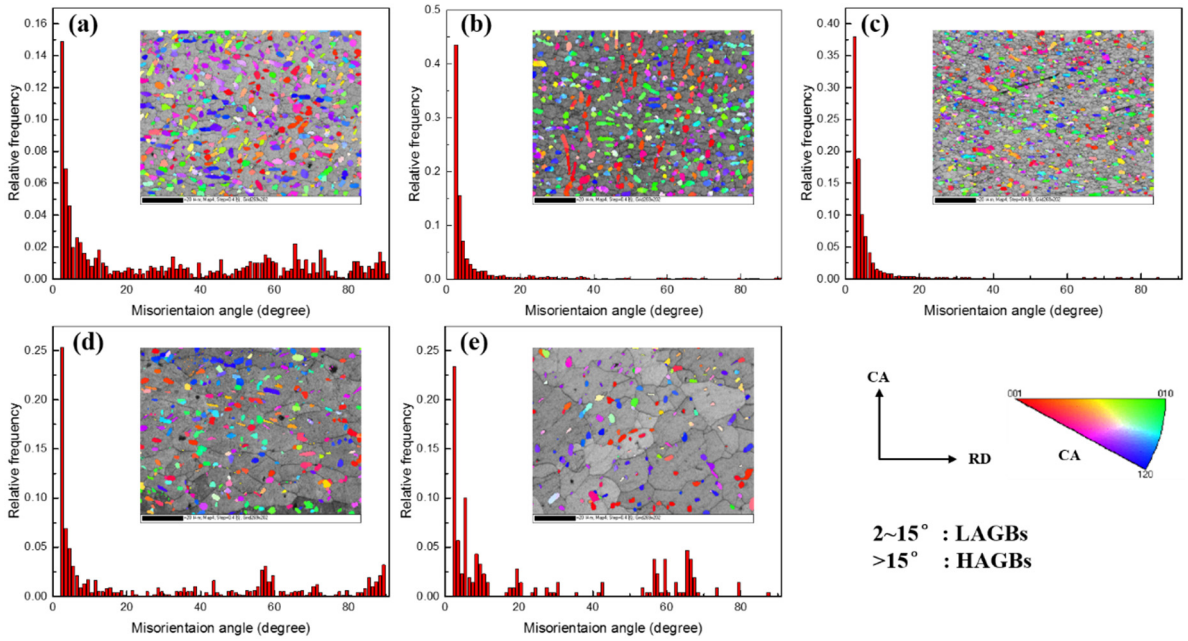

Figure 4. Distribution of grain boundary misorientation in the α phase for the deformed microstructure at different deformation conditions: (**a**) 740 °C/0.0001 s^{-1}; (**b**) 740 °C/0.01 s^{-1}; (**c**) 740 °C/1 s^{-1}; (**d**) 760 °C/0.0001 s^{-1}; (**e**) 780 °C/0.0001 s^{-1}.

3.2.2. β Recrystallization and β Microtexture Evolution

DRV usually occurs in the early deformation stage, in which the dislocations would be annihilated and easily rearranged as arrays. The result of DRV is the occurrence of LAGBs. The DRX is usually characterized by the formation of new strain-free fine grains. The two softening mechanisms are all significantly affected by the deformation conditions. Figure 5 gives the orientation distribution maps of the β phase at 740 °C and the different strain rates. The measured areas were located in the center of CA-RA planes, and the gray areas in the orientation maps represented α grains. Additionally, the areas indicated by the squares in Figure 5a–c are enlarged in Figure 5d–f. As a whole, the prior β grains were elongated along the RA direction, and the dynamic recovery and recrystallization occurred at all strain rates, characterized by the enriched β sub-grains, sporadically or chain-like distributed recrystallized β grains with a grain size far less than the prior β grains, and wave-shaped β grain boundaries. The continuous dynamic recrystallization (CDRX) can be considered as a dominant mechanism controlling the β phase microstructure evolution, which could be characterized by the new grains with HAGBs. The HAGBs could generate by the progressive rotation of sub-grains during the hot deformation [31]. The formation of HAGBs would be affected by the initial grain size, deformation conditions, and α phase evolution. Therefore, it can be seen that the β recrystallization is not homogeneous inside the prior β grains (Figure 5a–c).

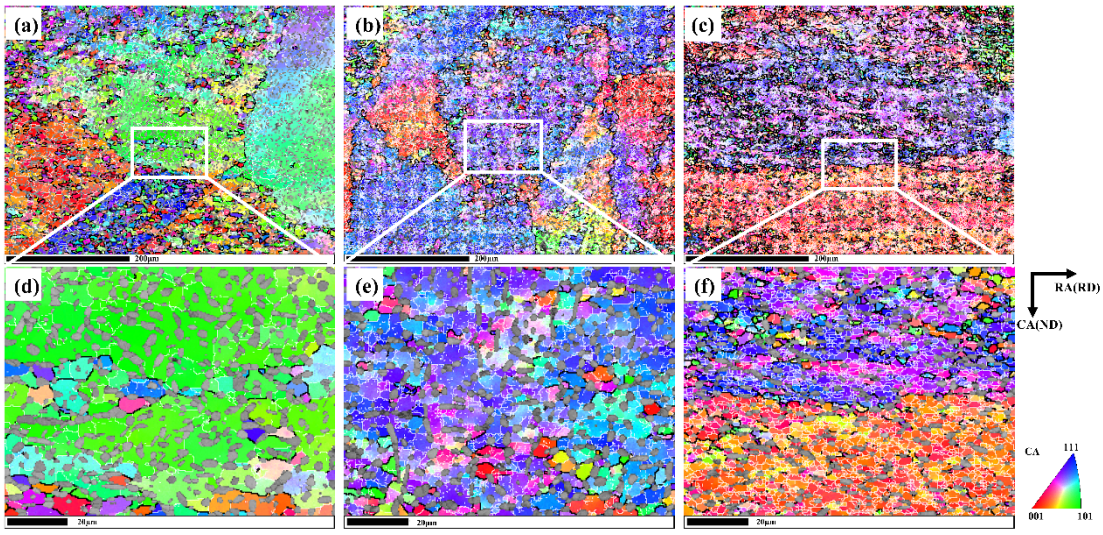

Figure 5. The IPF maps of the β phase in TB6 alloy deformed at 740 °C and varied strain rates: (**a**,**d**) 0.0001 s^{-1}; (**b**,**e**) 0.01 s^{-1}; (**c**,**f**) 1 s^{-1}.

The Kernel average misorientation maps (KAM) are calculated to investigate the geometrically necessary dislocations accumulated during hot deformation, which could reflect the local strain of different regions. As seen in Figure 6a–c, the regions colored with green and yellow expand with the strain rate increasing, which reflects the internal deformation and resultant microstructure evolution behavior. Notably, the KAM value is usually higher in the β/β boundaries and α/β phase boundaries, seen by comparing the IPF maps (Figure 5) and KAM maps (Figure 6). The high KAM values in the β/β boundaries can be attributed to the bcc crystallographic rotation and slip system activation. Additionally, under the strict Burgers orientation relationship, the slip transmission would be hindered at the α/β phase boundaries, leading to the high KAM values here. Figure 6d histogram illustrates the distribution of local misorientation average angles at different strain rates. It reflects the accelerated deformation hardening progress as the strain rate increases, which also demonstrates that the geometrically necessary dislocation (GND) evolution is closely related to plastic deformation and microstructural evolution. The evolution of the GND density could be reflected by the average KAM values. Therefore, the average KAM values are calculated. By calculation, the average KAM values in Figure 6a–c are 0.82, 1.43, and 1.58 (degree). It can be seen that the GND density would increase appreciably as the strain rates increased from 0.0001 s^{-1} to 0.01 s^{-1} and fluctuate slightly as the strain rates increased from 0.01 s^{-1} to 1 s^{-1}.

Generally, the loss of Burgers orientation relationship (BOR) between the α and β phase would give a wider latitude in the plastic deformation of the two phases, thus facilitating the slip deformation and consequently giving rise to the dislocation pile-ups. Wang et al. [32] reported that, under compressive deformation in the two phases field, the process of lamellae α fragmenting into the spherical ones was accompanied by the loss of BOR. Additionally, the efficiency of the morphology transformation mostly depends on the deviation degree of the BOR, which means that it plays a significant role in lamellar α evolution. It has been reported that the BOR would deteriorate with cumulative deformation amounts, and the results by Klimova et al. [33] showed that the total loss of BOR would occur as the true strain reached 1.2. It is reasonable for us to deduce that the β phase evolution would be significantly influenced under the strict BOR, especially for the deformation of α/β boundaries and its neighboring microstructure evolution. Therefore, considering the α/β phase boundaries restricted by the BOR, a detailed analysis was made to investigate the deviation of the ideal BOR with the strain rate increasing.

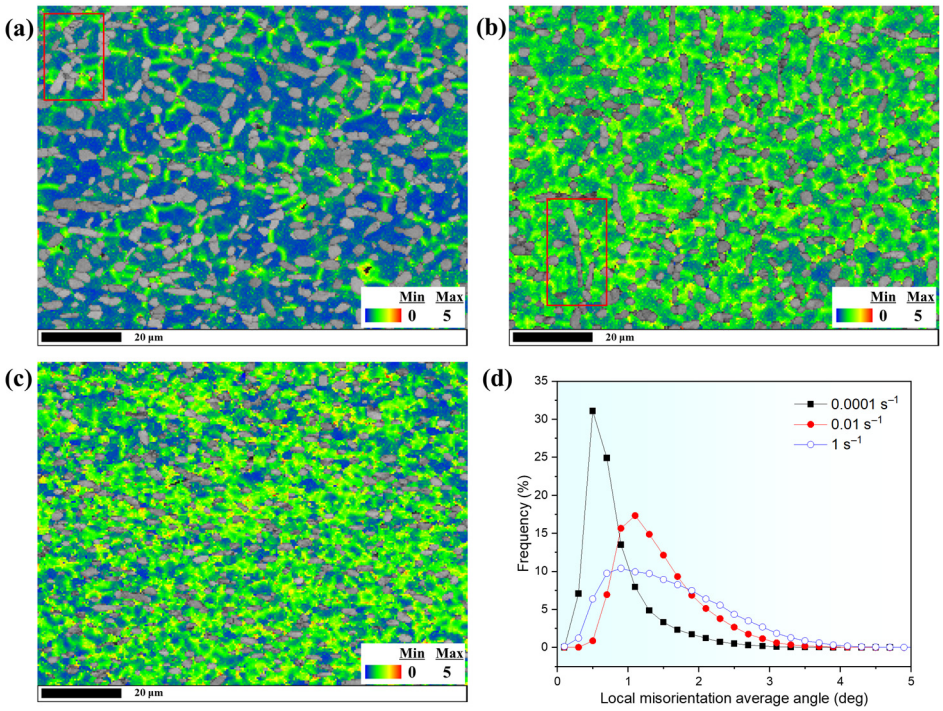

Figure 6. (**a**–**c**): the corresponding KAM maps of the β phase in Figure 3d–f; (**d**) the local misorientation distribution map.

The local areas identified by a red square marked in Figure 6a are enlarged in Figure 7a, as shown, where arrows A and C are the β phases, and arrow B is the neighboring α phase separated by the α/β phase boundaries. Differently, the KAM value in A is higher than that in C, and this varied misorientation along the α/β phase boundaries is common in other areas. In spite of this, the β phases at arrows A and C and the left adjacent α phase presented by arrow B obey the BOR well, as seen in Figure 7b–d. In Figure 7b,d, it could be explicitly observed that the bcc crystal structure in the adjacent β phase differs a lot, where the bcc crystal in C rotates 90 degrees about the [001] axis compared with the β phase in A. If this crystal rotation was motivated from deformation, it would give rise to the significant crystal orientation fluctuation, consequently producing the HAGBs inside the β phase here. However, no significant orientation fluctuation could be observed in Figure 5d. Therefore, the reason may be back to the variation selection during the α → β transformation process when the specimen was heating and holding. For the initial material that experienced hot forged processing in this paper, there are cumulative dislocations and defects in the microstructure. Therefore, the β variant selection may occur during the heating and holding before deformation, which consequently may affect the β phase evolution in hot deformation. Additionally, it can be seen that there is less deviation of the BOR between the β phase in arrow C and the α phase in arrow B, which reflects that the variation selection during the α → β transformation would affect the deformation of the β phase.

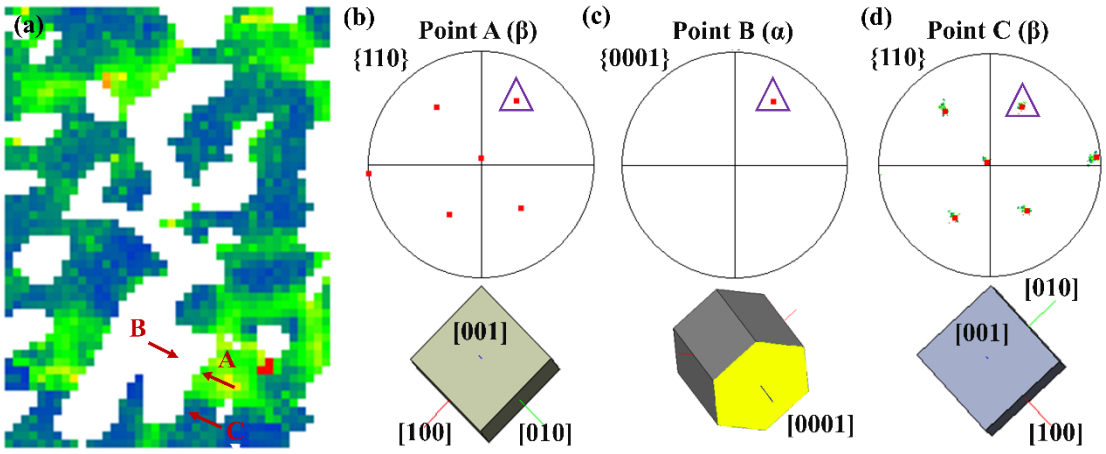

Figure 7. (**a**) The KAM values map of the β phase in local areas circled in Figure 4a; (**b**) the {110} β pole figure at arrow A; (**c**) the {0001} α pole figure at arrow B; (**d**) the {110} β pole figure at arrow C.

As demonstrated in Figure 6, as the strain rate increases, the integral KAM values and the proportion of the average misorientation angles higher than 1° both have an increment. Additionally, the average misorientation distribution of the β phase in the local areas indicated by a red square marked in Figure 6b is exhibited in Figure 8a. The {110} β pole figures at arrows A and C can be seen in Figure 8b,d. The corresponding {0001} α pole figure at the adjacent α phase at arrow B is exhibited in Figure 8c. The prior equiaxed α phase (arrow B) and its neighboring β phase (arrows A and C) obey the BOR (Figure 8b–d). According to the corresponding crystal structure relationship, the slip planes of the α and β phases satisfy a certain relationship $(0001)_\alpha//\{110\}_\beta$, $\{0{-}110\}_\alpha//\{1{-}12\}_\beta$ and $\{0{-}111\}_\alpha//\{01{-}1\}_\beta$. Furthermore, the <11−20> α slip direction keeps parallel to the <111> β slip direction. It is accepted that the dislocation slip transmission across the α/β phase boundaries would be promoted given that the slip systems of the constitutive phase were in good geometric alignment [33]. According to their investigation, it can be known that the slip systems of the β phase would be notably activated through slip transmission under a certain condition. This can occur when the slip system of the β phase and the most active slip system of the α phase hold a collinear slip relation. The phenomenon that dislocations are concentrated at the phase boundaries (arrow A) suggests that, even under the BOR (Figure 8b,c), the slip transmission at the interfaces is difficult due to the non-collinear slip relation of slip systems of the two phases [34].

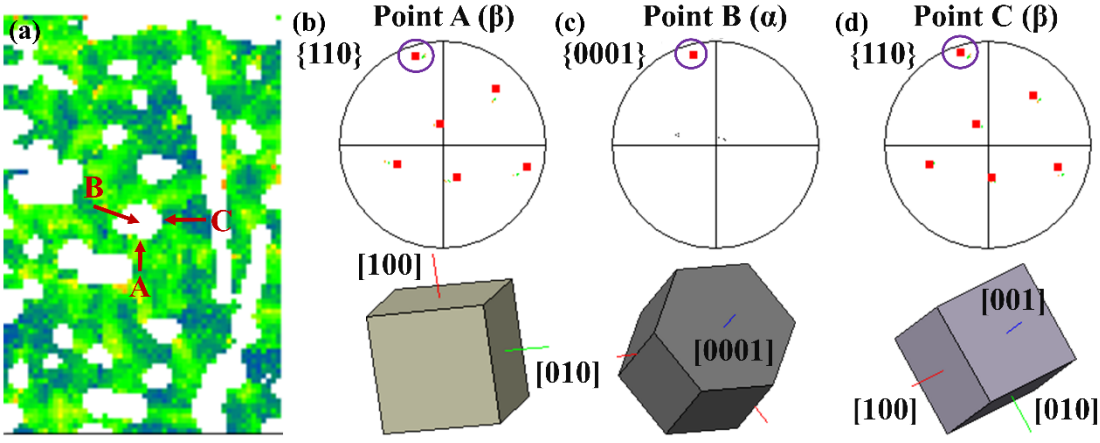

Figure 8. (**a**) The KAM values map of the β phase in local areas circled in Figure 4b; (**b**) the {110} β pole figure at arrow A; (**c**) the {0001} α pole figure at arrow B; (**d**) the {110} β pole figure at arrow C.

As for arrow C, it rotates a lot compared with the β phase in arrow A, and the KAM value in arrow C is lower, which means that the slip transmission here was not hindered. The activation of slip transmission would affect the texture evolution in the β phase, which is worthy of further exploration. In addition, the significant α grain rotation in arrow C cannot be overlooked, and consequently resulted in the HAGBs, as shown in Figure 5e. However, such a severe grain rotation did not destroy the BOR between the two phases, which indicates that the orientation evolution of the β phase is conditioned by the BOR. Further, under the circumstances, the strong β microtexture with various components would form easily.

According to the characterization results above, the recrystallized β grains with a small grain size could be found at the initial α grain boundaries or inside the β matrix. Figure 9 shows the distribution of the grain boundary misorientation in the β phase for the deformed microstructure and the corresponding IPF maps at different deformation conditions. It can be seen that the fraction of HAGBs at a lower strain is significant high, which could reflect the recrystallization fraction, i.e., the recrystallization would be promoted with decreasing the strain rate. To further verify the result, the distribution of the grain boundary misorientation in the β phase at other deformations can be seen in Figure 10. The fractions of HAGBs at each deformation temperature are high and the distribution of HAGBs is significantly heterogeneous. The β recrystallization grains are inlaid inside the β matrix, in which they show an aggregation distribution at a lower strain rate and a dispersed distribution at a higher strain rate. Li et al. [35] reported that the DRX would enhance with the strain rate increasing due to the accumulated dislocations, i.e., there would be a more sufficient driving force for the LAGBs transforming into the HAGBs. However, as the DRX is also a time-consuming process, there would be limited opportunities for the recrystallized β grains to further grow up and extend if the strain rate was higher.

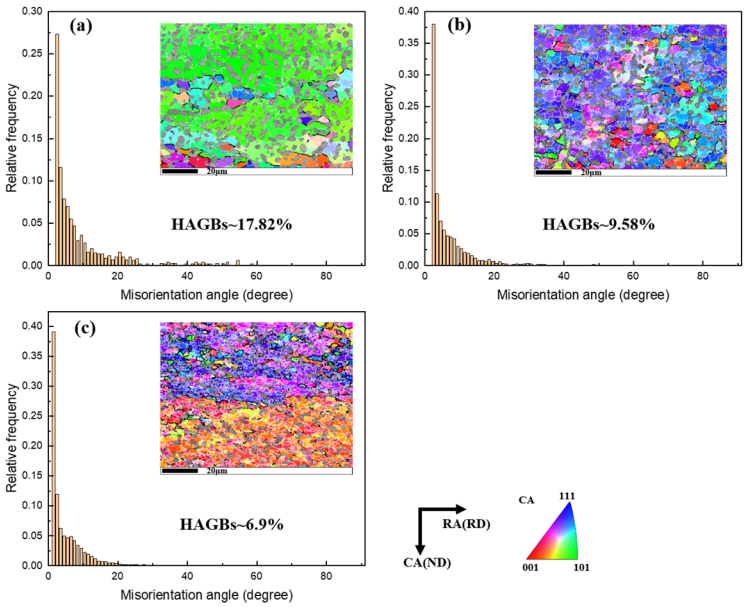

Figure 9. Distribution of the grain boundary misorientation in the β phase for the deformed microstructure and the corresponding IPF maps at different deformation conditions: (**a**) 740 °C/0.0001 s^{-1}; (**b**) 740 °C/0.01 s^{-1}; (**c**) 740 °C/1 s^{-1}.

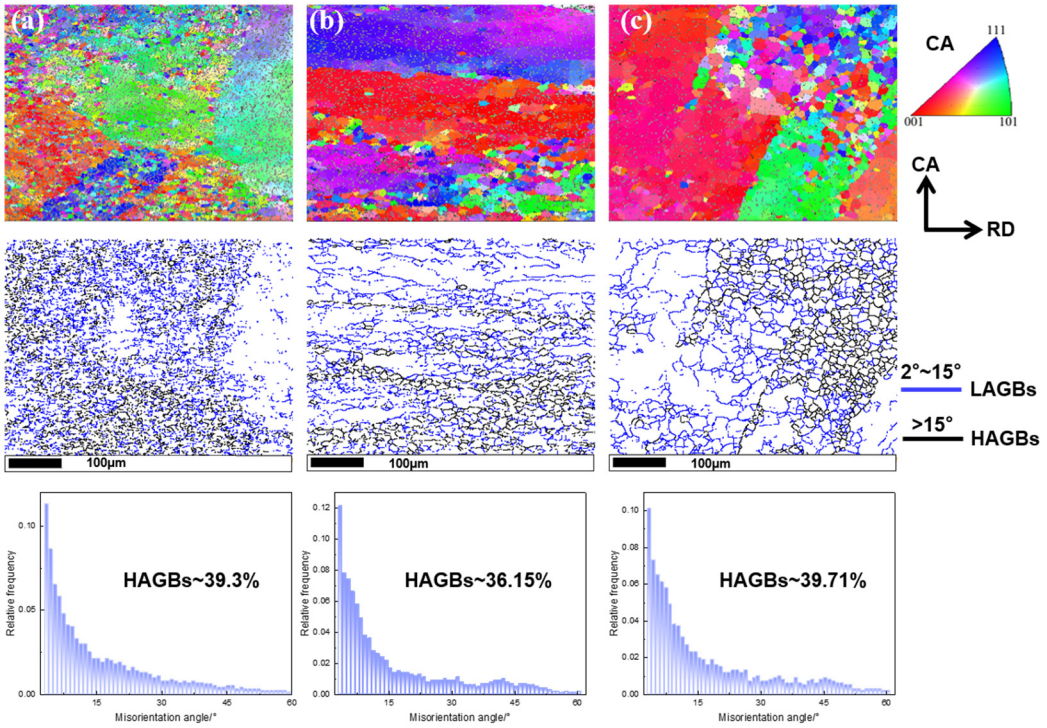

Figure 10. Distribution of the grain boundary misorientation in the β phase for the deformed microstructure and the corresponding IPF maps at different deformation conditions: (**a**) 740 °C/0.0001 s^{-1}; (**b**) 760 °C/0.0001 s^{-1}; (**c**) 780 °C/0.0001 s^{-1}.

As shown in Figures 5 and 10, the deformed β phase with a dynamic recovered state occupied a large fraction in the matrix, which may dominate the texture components and their intensity after deformation. According to Figure 5, the IPFs of sub-structured and deformed grains and recrystallized β grains were further calculated to analyze the β microtexture characteristics at different deformation conditions, which can be seen in Figure 11. From the above results, it can be observed that the β microtexture is significant. It can be interpreted by the fact that the β recrystallization would inherit the microtexture components of the sub-structured and deformation grains to some extent, and this phenomenon is more significant at the strain rate of 0.0001 s^{-1}.

The intensity and components of microtexture are different at different conditions. When the strain rate was 0.0001 s^{-1}, the β recrystallization phase and sub-structured and deformed grains displayed a simple <001>//RD fiber microtexture component. The <001>//RD microtexture was found in β titanium alloys after compression deformation, which would deteriorate the mechanical properties of the final products.

It has been reported that the occurrence of β recrystallization would further strengthen the microtexture and its intensity would increase with the strain increasing [36], which were both observed in the forging process in the β single-phase region. A weak <102>//RD microtexture could be observed both within the recrystallized β grains and the sub-structured and deformed β matrix when the strain rate was 0.01 s^{-1}. On the other hand, the recrystallized β grains showed a more significant orientation spread than the sub-structured and deformed matrix. Two kinds of orientation concentration for the recrystallized and deformed microstructure could be seen when the strain rate reached 1 s^{-1}. This is because two initial β grains with different crystallographic orientations were included in the scanning area, as shown in Figure 5c. By comparison, it seems that the orientation of β recrystallization did not solely present the "inheritance" characteristic, and the β microtexture intensity would be weakened due to the occurrence of some β recrystallization grains with no-preferred orientation. The differences in microtexture components and intensity may be affected by initial orientation, β recrystallization, and deformation conditions. Therefore, the operated β slip systems need to be discussed further.

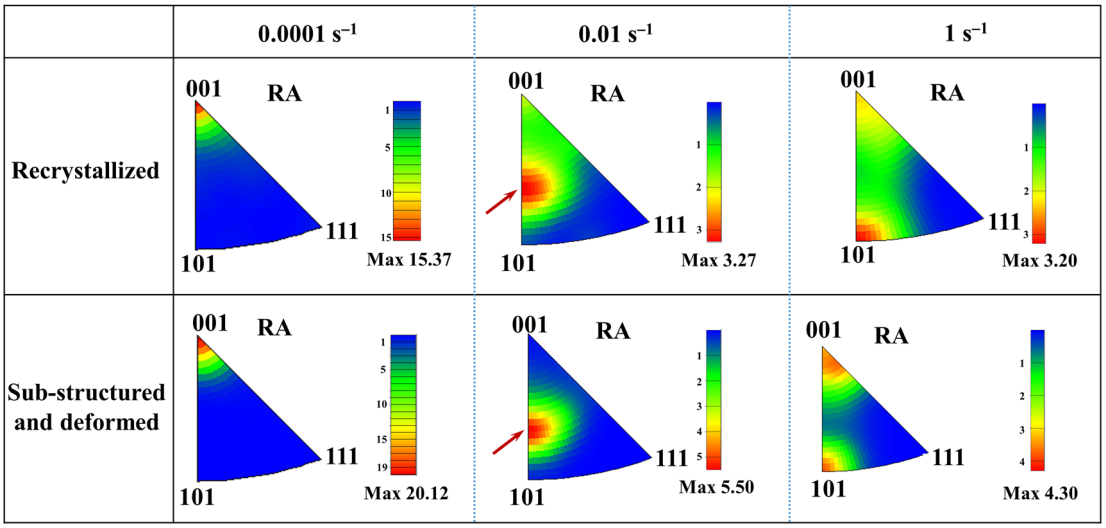

Figure 11. The IPFs of the recrystallized β phase and the sub-structured and deformed β phase at various strain rates.

3.2.3. The Activity of β Slip Systems during Deformation

The operating of slip systems finally affected the microtexture intensity. During deformation, the activity of slip systems depends on the Schmid factor (SF) and the critical resolved shear stress (CRSS). For the β phase in titanium alloys, the {1−10}<111>, {11−2}<111>, and {12−3}<111> slip systems are perceived as the active ones at high temperatures. Among them, the activity of the {1−10}<111> slip system would result in a weak {001} and a sharp {111} texture; whereas the {11-2}<111> and {12-3}<111> slip systems tend to generate a {111} and {001} β texture, respectively [16,27]. Figure 12 shows the Schmid factor maps for the {1−10}<111> slip system, in which the SF value is calculated relative to the CA. The corresponding distributions of SF values for the {1−10}<111>, {11−2}<111>, and {12−3}<111> slip systems can be seen in Figure 13. At a lower strain rate, the {1−10}<111> slip system is highly activated, in which the SF value of the β phase is mostly larger than 0.4 (Figure 12a,b). However, as shown in Figure 12c, there is a significant differentiated distribution of the SF value in the two regions (the two adjacent initial β grains). The SF values in the top region of the image are commonly less than 0.4, which is more significant within the un-recrystallized β grains.

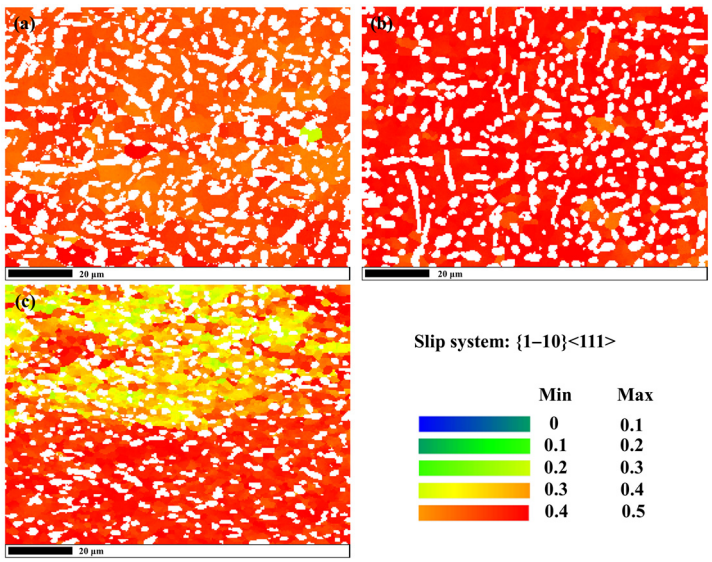

Figure 12. Schmid factor maps for the {1−10} <111> slip system of TB6 titanium alloy deformed at 740 °C and different strain rates: (**a**) 0.0001 s^{-1}; (**b**) 0.01 s^{-1}; (**c**) 1 s^{-1}.

At 0.0001 s^{-1}, the highest frequency SF value on the {110}<111> slip system is ~0.435 (see the peak point on the black curve in Figure 13a), and this value is markedly lower than that at 0.01 s^{-1}. However, the case is contrary for the SF value distribution on the {11−2}<111> and {12−3}<111> slip systems, i.e., the highest frequency SF values are ~0.495 and 0.485, respectively, at the stain rate of 0.0001 s^{-1} (seen in Figure 13b,c), which are higher than that at 1 s^{-1} and 0.01 s^{-1}. Therefore, the higher activity of the {11−2}<111> and {12−3}<111> slip systems enhanced the <001>//RD β microtexture, as shown in Figure 12.

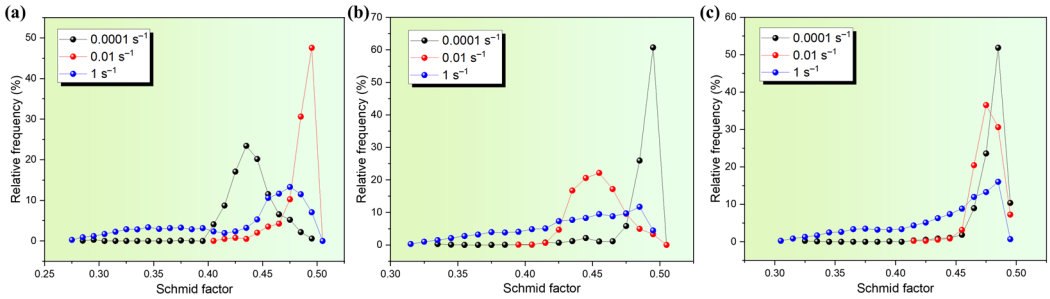

Figure 13. Relative frequency of SF values for different slip systems of TB6 titanium alloy compressed at 740 °C and different strain rates: (**a**) {1−10}<111>; (**b**) {11−2}<111>; (**c**) {12−3}<111>.

To further determine if the β grains rotated along the axes of some special interfaces, the maps of Rot. Axes in crystal CS0 were plotted, as shown in Figure 14. The weak rotation axes had a multiple uniform distribution (mud) of less than 2 on the standard unit triangle, which hints that the deformed grains experienced a slight lattice rotation. However, in this work, it would be considered to take on the preferred in-grain misorientation axes when the maximum intensity was higher than 2, which is consistent with the definition in the literature by Chun et al. [37]. It is noted that the distribution of the rotation axes of 2~15° boundaries in the β phase is not concentrated toward a certain axis, showing a maximum intensity lower than 1.3 at any strain rate. It indicates that the rotation of 2~15° boundaries was nearly unaffected by the strain rate. For the boundaries with high angles of 15~75°, the rotation axes show a non-uniform distribution at 0.01 s^{-1} and 0.0001 s^{-1}, the intensities of which are not negligible around the <101> axis, unlike the case for the 2~15° boundaries. As the strain rate increases to 1 s^{-1}, strong intensities around the <101> axis cannot be observed, showing a relatively uniform distribution.

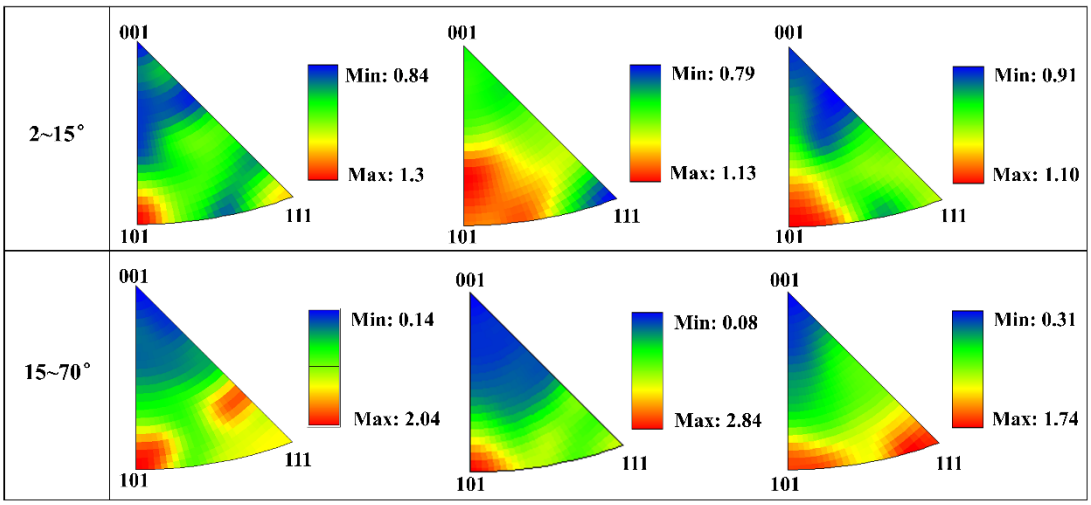

Figure 14. The rotation axes distribution for the deformed grains shown in Figure 5.

At 0.0001 s^{-1}, the operation of the {11−2}<111> and {12−3}<111> slip systems induced the crystal rotation around <101>, but such crystal rotation did not destroy the

BOR between the two constituent phases. The result is that some β/β boundaries with misorientation angles less than 15° would form inside the deformed β matrix. Additionally, these β/β boundaries would further transform into the HAGBs with deformation proceeding. The low β recrystallization fraction and the crystallographic inheritance of the recrystallized β grains on the adjacent matrix account for the strong β microtexture after hot compression. With the strain rate increasing to 0.01 s^{-1}, dislocation multiplication increases, and the fraction of LAGBs also increases. According to the experimental result, we could conclude that the {1−10}<111> and {12−3}<111> slip systems are activated during deformation, consequently decreasing the <001>//RD microtexture and generating the <102>//RD microtexture. Based on the multiple characterization results above, it can be concluded that the CDRX is the main mechanism controlling the recrystallization process inside β grains. When the strain rate was higher, the dislocation glide would be a dominant deformation mechanism, and some divergences on the operation of slip systems in two β grains with different orientations lead to a relatively weak microtexture and a lower value in rotation axes mud.

4. Conclusions

This research focuses on the β-phase evolution characteristics of TB6 titanium alloy during (α + β) dual-phase field isothermal compression, which was undertaken by the electron backscatter diffraction technique. Some main conclusions could be drawn from above experimental results analysis.

1. The β recrystallization is not homogeneous among prior β grains, and is characterized by enriched β sub-grains, sporadically or chain-like distributed recrystallized β grains with a grain size far less than the prior β grains, and wave-shaped β grain boundaries. The fraction of HAGBs would increase with the strain rate decreasing, whereas the average grain size and the volume fraction of the α phase are relatively stable with the strain rate varying. The CDRX is the main mechanism controlling the recrystallization process inside β grains and it is more significant at a lower strain rate.
2. The prior, coarse β grains are difficult to effectively transform into fine grains with random crystallographic orientations by an axial compression deformation in the (α + β) field, which is reflected in the orientation inheritance of recrystallized β grains. A significant β microtexture could be observed in the deformed microstructure. The β recrystallization microtexture did not solely present the "inheritance" characteristic, and its intensity would be weakened to a certain extent due to the occurrence of some recrystallization grains with no-preferred orientation.
3. When the strain rate was 0.0001 s^{-1}, the operation of the {11−2}<111> and {12−3}<111> slip systems would induce the crystal rotation around <101>, but such crystal rotation does not destroy the BOR between the two constituent phases, which may be the main reason that is causing the formation of a strong β microtexture. With the increasing the strain rate, the {1−10}<111> and {12−3}<111> slip systems are activated during deformation, consequently weakening the <001>//RD microtexture.

Author Contributions: Data curation, D.S. and L.W.; Funding acquisition, Q.C.; Investigation, Y.Y. and R.W.; Writing—original draft, D.S.; Writing—review and editing, L.W. and M.L. All authors have read and agreed to the published version of the manuscript.

Funding: The authors are grateful for funding support from National Natural Science Foundation of China (5207052610) and State Key Lab for Advanced Metals and Materials of China (2019-ZD04).

Institutional Review Board Statement: Not applicable.

Informed Consent Statement: Not applicable.

Data Availability Statement: The data that support the findings of this study are available from the corresponding author upon reasonable request.

Conflicts of Interest: The authors declare that they have no known competing financial interest or personal relationships that could have appeared to influence the work reported in this paper.

References

1. Ferrero, J.G. Candidate materials for high-strength fastener applications in both the aerospace and automotive industries. *J. Mater. Eng. Perform.* **2005**, *14*, 691–696. [CrossRef]
2. Kolli, R.P.; Devaraj, A. A review of metastable beta titanium alloys. *Metals* **2018**, *8*, 506. [CrossRef]
3. Boyer, R.R. Attributes, characteristics, and applications of titanium and its alloys. *Jom-US* **2010**, *62*, 21–24. [CrossRef]
4. Boyer, R.R.; Briggs, R.D. The use of β titanium alloys in the aerospace industry. *J. Mater. Eng. Perform.* **2005**, *14*, 681–685. [CrossRef]
5. Srinivasu, G.; Natraj, Y.; Bhattacharjee, A.; Nandy, T.K.; Nageswara Rao, G.V.S. Tensile and fracture toughness of high strength β titanium alloy, Ti–10V–2Fe–3Al, as a function of rolling and solution treatment temperatures. *Mater. Des.* **2013**, *47*, 323–330. [CrossRef]
6. Ma, X.; Chen, Z.; Xiao, L.; Luo, S.; Lu, W. Stress-induced martensitic transformation in a β-solution treated Ti–10V–2Fe–3Al alloy during compressive deformation. *Mater. Sci. Eng. A* **2021**, *801*, 140404. [CrossRef]
7. Lei, X.; Dong, L.; Zhang, Z.; Liu, Y.; Hao, Y.; Yang, R.; Zhang, L.C. Microstructure, texture evolution and mechanical properties of VT3-1 titanium alloy processed by multi-pass drawing and subsequent isothermal annealing. *Metals* **2017**, *7*, 131. [CrossRef]
8. Li, J.S.; Dong, R.F.; Kou, H.C.; Fan, J.K.; Zhu, B.; Tang, B. Texture evolution and the recrystallization behavior in a near β titanium alloy Ti-7333 during the hot-rolling process. *Mater. Charact.* **2020**, *159*, 109999. [CrossRef]
9. Levkulich, N.C.; Semiatin, S.L.; Payton, E.J.; Srivatsa, S.; Pilchak, A.L. An investigation of the development of coarse grains during β annealing of hot-forged Ti-6Al-4V. *Metall. Mater. Trans. A Phys. Metall. Mater. Sci.* **2021**, *52*, 1353–1367. [CrossRef]
10. Fan, X.G.; Zhang, Y.; Gao, P.F.; Lei, Z.N.; Zhan, M. Deformation behavior and microstructure evolution during hot working of a coarse-grained Ti-5Al-5Mo-5V-3Cr-1Zr titanium alloy in beta phase field. *Mater. Sci. Eng. A* **2017**, *694*, 24–32. [CrossRef]
11. Syed, F.W.; Jaladurgam, N.R.; Kumar, V.A.; Gupta, R.K.; Kanjarla, A.K. Hot deformation characteristics and microstructure evolution of Ti–5Al–3Mo–1.5V alloy. *Int. J. Adv. Eng. Sci. Appl. Math.* **2021**, *13*, 49–62. [CrossRef]
12. Germain, L.; Gey, N.; Humbert, M.; Bocher, P.; Jahazi, M. Analysis of sharp microtexture heterogeneities in a bimodal IMI 834 billet. *Acta Mater.* **2005**, *53*, 3535–3543. [CrossRef]
13. Gey, N.; Bocher, P.; Uta, E.; Germain, L.; Humbert, M. Texture and microtexture variations in a near-α titanium forged disk of bimodal microstructure. *Acta Mater.* **2012**, *60*, 2647–2655. [CrossRef]
14. Fan, X.G.; Zheng, H.J.; Zhang, Y.; Zhang, Z.Q.; Gao, P.F.; Zhan, M.; Liu, J. Acceleration of globularization during interrupted compression of a two-phase titanium alloy. *Mater. Sci. Eng. A* **2018**, *720*, 214–224. [CrossRef]
15. Wang, L.; Fan, X.G.; Zhan, M.; Jiang, X.Q.; Zeng, X.; Liang, Y.F.; Zheng, H.J.; Zhao, A.M. The heterogeneous globularization related to crystal and geometrical orientation of two-phase titanium alloys with a colony microstructure. *Mater. Des.* **2020**, *186*, 108338. [CrossRef]
16. Meng, L.; Kitashima, T.; Tsuchiyama, T.; Watanabe, M. β-Texture evolution during α precipitation in the two-step forging process of a near-β titanium alloy. *Metall. Mater. Trans. A Phys. Metall. Mater. Sci.* **2020**, *51*, 5912–5922. [CrossRef]
17. Corre, S.L.; Forestier, R.; Brisset, F.; Mathon, M.-H.; Solas, D. Influence of β-forging on texture development in Ti6246 alloy. In Proceedings of the 13th World Conference on Titanium, San Diego, CA, USA, 16–20 August 2016; pp. 757–764. [CrossRef]
18. Fan, J.K.; Kou, H.C.; Lai, M.J.; Tang, B.; Chang, H.; Li, J.S. Characterization of hot deformation behavior of a new near beta titanium alloy: Ti-7333. *Mater. Des.* **2013**, *49*, 945–952. [CrossRef]
19. Fan, J.K.; Kou, H.C.; Lai, M.J.; Tang, B.; Chang, H.; Li, J.S. Hot deformation mechanism and microstructure evolution of a new near β titanium alloy. *Mater. Sci. Eng. A* **2013**, *584*, 121–132. [CrossRef]
20. Ning, Y.Q.; Luo, X.; Liang, H.Q.; Guo, H.Z.; Zhang, J.L.; Tan, K. Competition between dynamic recovery and recrystallization during hot deformation for TC18 titanium alloy. *Mater. Sci. Eng. A* **2015**, *635*, 77–85. [CrossRef]
21. Hua, K.; Xue, X.Y.; Kou, H.C.; Fan, J.K.; Tang, B.; Li, J.S. Characterization of hot deformation microstructure of a near beta titanium alloy Ti-5553. *J. Alloys Compd.* **2014**, *615*, 531–537. [CrossRef]
22. Hua, K.; Zhang, Y.; Gan, W.; Kou, H.C.; Beausir, B.; Li, J.S. Hot deformation behavior originated from dislocation activity and β to α phase transformation in a metastable β titanium alloy. *Int. J. Plast.* **2019**, *119*, 200–214. [CrossRef]
23. Chen, J.H.; Li, J.S.; Tang, B.; Chen, Y.; Kou, H.C. Microstructure and texture evolution of a near β titanium alloy Ti-7333 during continuous cooling hot deformation. *Prog. Nat. Sci. Mater.* **2019**, *29*, 50–56. [CrossRef]
24. Su, J.; Sanjari, M.; Kabir, A.S.H.; Jung, I.; Yue, S. Dynamic recrystallization mechanisms during high speed rolling of Mg-3Al-1Zn alloy sheets. *Scr. Mater.* **2016**, *113*, 198–201. [CrossRef]
25. Li, L.; Li, M.Q.; Luo, J. Mechanism in the β phase evolution during hot deformation of Ti–5Al–2Sn–2Zr–4Mo–4Cr with a transformed microstructure. *Acta Mater.* **2015**, *94*, 36–45. [CrossRef]
26. Beausir, B.; Fundenberger, J.-J. *Analysis Tools for Electron and X-Ray Diffraction, ATEX—Software, Version 2007*; Université de Lorraine: Metz, France, 2017.
27. Meng, L.; Kitashima, T.; Tsuchiyama, T.; Watanabe, M. β-Texture evolution of a near-β titanium alloy during cooling after forging in the β single-phase and (α + β) dual-phase regions. *Metall. Mater. Trans. A Phys. Metall. Mater. Sci.* **2021**, *52*, 303–315. [CrossRef]

28. Jackson, M.; Dashwood, R.; Christodoulou, L.; Flower, H. The microstructural evolution of near beta alloy Ti-10V-2Fe-3Al during subtransus forging. *Metall. Mater. Trans. A* **2005**, *36*, 1317–1327. [CrossRef]
29. Warchomicka, F.; Poletti, C.; Stockinger, M. Study of the hot deformation behaviour in Ti–5Al–5Mo–5V–3Cr–1Zr. *Mater. Sci. Eng. A* **2011**, *528*, 8277–8285. [CrossRef]
30. Lin, Y.C.; Huang, J.; He, D.G.; Zhang, X.Y.; Wu, Q.; Wang, L.H.; Chen, C.; Zhou, K.C. Phase transformation and dynamic recrystallization behaviors in a Ti55511 titanium alloy during hot compression. *J. Alloys Compd.* **2019**, *795*, 471–482. [CrossRef]
31. Gourdet, S.; Montheillet, F. An experimental study of the recrystallization mechanism during hot deformation of aluminium. *Mater. Sci. Eng. A* **2000**, *283*, 274–288. [CrossRef]
32. Wang, L.; Fan, X.G.; Zhan, M.; Jiang, X.Q.; Liang, Y.F.; Zheng, H.J.; Liang, W.J. Revisiting the lamellar globularization behavior of a two-phase titanium alloy from the perspective of deformation modes. *J. Mater. Process. Technol.* **2021**, *289*, 116963. [CrossRef]
33. Klimova, M.; Zherebtsov, S.; Salishchev, G.; Semiatin, S.L. Influence of deformation on the Burgers orientation relationship between the α and β phases in Ti–5Al–5Mo–5V–1Cr–1Fe. *Mater. Sci. Eng. A* **2015**, *645*, 292–297. [CrossRef]
34. Savage, M.F.; Tatalovich, J.; Mills, M.J. Anisotropy in the room-temperature deformation of α-β colonies in titanium alloys: Role of the α-β interface. *Philos. Mag.* **2004**, *84*, 1127–1154. [CrossRef]
35. Li, L.; Luo, J.; Yan, J.J.; Li, M.Q. Dynamic globularization and restoration mechanism of Ti–5Al–2Sn–2Zr–4Mo–4Cr alloy during isothermal compression. *J. Alloys Compd.* **2015**, *622*, 174–183. [CrossRef]
36. Meng, L.; Kitashima, T.; Tsuchiyama, T.; Watanabe, M. Effect of α precipitation on β texture evolution during β-processed forging in a near-β titanium alloy. *Mater. Sci. Eng. A* **2020**, *771*, 138640. [CrossRef]
37. Chun, Y.B.; Battaini, M.; Davies, C.H.J.; Hwang, S.K. Distribution characteristics of in-grain misorientation axes in cold-rolled commercially pure titanium and their correlation with active slip modes. *Metall. Mater. Trans. A Phys. Metall. Mater. Sci.* **2010**, *41*, 3473–3487. [CrossRef]